17th Australasian Fluid Mechanics Conference
Auckland, New Zealand
5-9 December 2010

Numerical Simulation of a Supersonic Convergent Divergent Nozzle with divergent angle variations for Underexpanded condition

E.M. S. Ekanayake[1], J. A. Gear[2] and Y. Ding[3]

[1]School of Mathematical and Geospatial Sciences
RMIT University, Victoria 3001, Australia

[2]School of Mathematical and Geospatial Sciences
RMIT University, Victoria 3001, Australia

[3]School of Mathematical and Geospatial Sciences
RMIT University, Victoria 3001, Australia

Abstract

Flow through a two-dimensional supersonic Convergent-Divergent nozzle with a rectangular cross section is investigated. The numerical simulation is modeled for three geometry shapes, NAR (Nozzle Area Ratio A_e/A_t) 1.5, 1.14 and 1.21 adding an angle variation to the divergent section for NAR 1.14 and 1.21.

Computation is carried out for low NPRs (Nozzle Pressure Ratio) between 1.27 and 2.4 and high NPRs between 4.4 and 12. Ambient pressure and temperature of 4375Pa (0.04317atm) and 228K is simulated under 18-20km altitude conditions to observe the shock formations within the jet plume region. The computation is solved with Reynolds Average Navier-Stokes Equations inbuilt to ANSYS-CFX solver with the SST Turbulence model.

Axisymmetric two dimensional nozzle, NAR 1.5 is compared with asymmetric models of NAR 1.14 and 1.21 under high NPRs. The nozzle NAR is varied to investigate the flow direction and speed of the gas, for nozzle underexpanded condition. Numerical computation is mainly focused on nozzles operating at high NPR to investigate the formation of the jet plume shocks and direction of the expanding gas. Nozzle with NAR 1.21 the path of the exhaust gas flow has diverted significantly compared to NAR 1.14.

Introduction

Supersonic convergent divergent (CD) nozzles are used not only on military jet exhausts but also significantly on current high speed missiles. The shape of the nozzle/diffuser is the key to the expansion process. It plays a vital part towards designing the flow, minimizing thrust loss by expanding the gas to its maximum potential. Proven to expand gas more efficiently than a nozzle with a circularly contoured cross section, the jet nozzle with a rectangular cross section is modeled during this analysis [1, 2, 3].

To obtain maximum thrust at a given pressure ratio, theoretically the exit pressure should be equal to the external ambient pressure. Jet aircrafts fly at high altitudes, as decreased pressure and temperature, requires less expansion of the exhaust gas. It is customary to design the nozzle to operate at a given altitude. At higher altitudes the exhaust gas is underexpaned and overexpanded at sea-level conditions.

When the exit pressure (gas) of the divergent section of the nozzle is different from the external ambient pressure flow undergoes several phenomena depending on the nozzle pressure ratio. Some experimental and computational simulations have been done for gas emerging through a CD nozzle under low NPRs . These investigations were mainly focused on the mixing enhancement for potential applications towards fuel injection and thermal signature reductions in jet engine fuel systems for NAR 1.5 [4, 5]. Other computational studies analyzed, the effects of pressure, aspect ratio and Mach numbers for nozzles with NPR less than 3 [6].

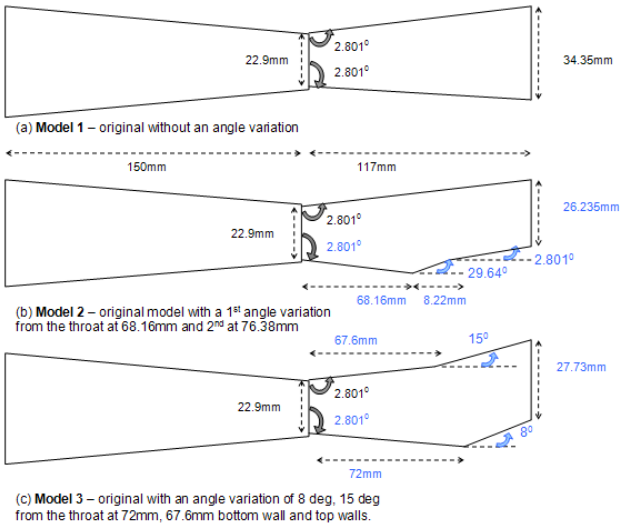

Figure 1: Geometry set-up (a)Model 1(NAR 1.5), (b)Model 2 (NAR 1.14), (c)Model 3 (NAR 1.21).

Flow Separation and Plume Instability

When the static pressure is increased, an adverse pressure gradient causes the boundary layer to detach from the nozzle wall surface. This increase in static pressure which contributes to increased potential energy of the gas thereby decreases the kinetic energy of the flow. The inner layer of the boundary, which is relatively slow, is significantly affected by this adverse pressure gradient and flow reversal may occur. The phenomena of flow reversal causes the flow to separate from the surface creating a circulation bubble [7]. Shocks emerging from the boundary layer start as an incident shock, reflect as a reflection shock, meeting at a triple point. This shock structure is called Lambda foot.

Over-expansion occurs at low to medium NPRs. The pressure at the exit of the nozzle (back pressure) is less than ambient pressure causing the Normal shock wave to bend towards the jet plume. The shock wave is oblique to the wall forming a complex flow pattern exiting the nozzle as a combination of

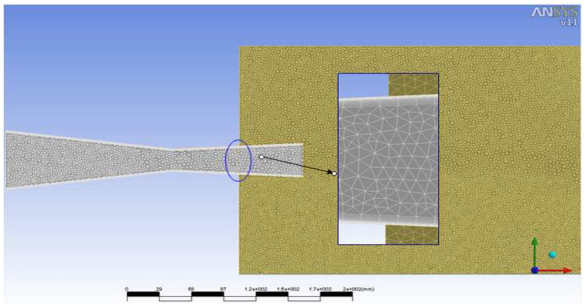

Figure 2: Mesh close-up for Model 1 with total no of 77,035 medium unstructured elements.

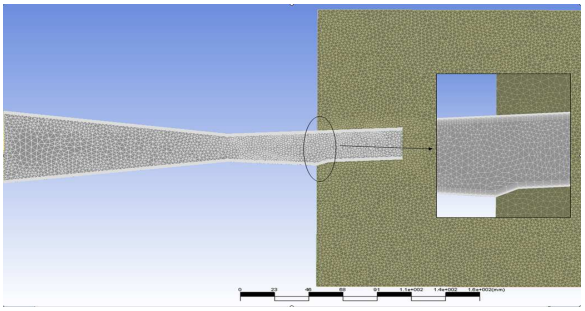

Figure 3: Mesh close-up for Model 2 with total no of 187,767 fine unstructured elements.

subsonic and supersonic flows. Further increasing NPR causes the back pressure to match the ambient pressure, resulting in a smooth flow, uniform supersonic and parallel. This is the ideal design condition [7]. Increasing the pressure further (exit pressure now greater than ambient) creates a new imbalance, where the waves at the exit of the nozzle wall turn outward as expansion waves, creating a new flow pattern where compression and expansion waves repeat downstream along the plume region (Under-expanded condition).

Nozzle Geometry Models and Computational Setup

Geometry of the nozzles

A two dimensional nozzle with a rectangular cross section [7] is modeled in ANSYS CFX software Package. ANSYS CFX is a conservative Finite Element (FE) based control volume method which uses implicit pressure-based algorithm for all flow speeds, from incompressible to compressible (subsonic/transonic/supersonic). The advection modeling is done using upwind differencing scheme with 1st and 2nd order blend factors. The nozzle non-variable convergent length and angle are 150mm and 7deg (see figure 1(a)). In the three test models the throat height is constant at 22.9mm. The second model has a variation in the divergent section (see figure 1(b)) with first and second angle variation of 29.64 and 2.801 degs from the throat at 68.16mm, and 2nd at 76.38mm. The third model has an angle variation of 8 deg, 15 deg from the throat at 72mm, 67.6mm bottom wall and top walls respectively (see figure 1(c)). Total divergent length of 117mm remains consistent for all three models. The geometry is set as a combination of two regions: the nozzle region and a external plume region to capture instabilities of the gas emerging from the throat to the jet plume region (see figures 2,3,4).

The NAR 1.14 with two angle variation to the bottom wall and NAR 1.21 with both walls are used to observe the flow direction

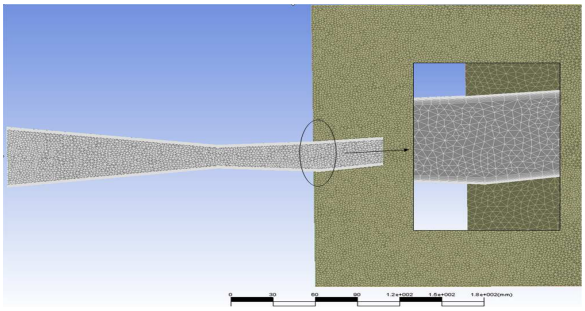

Figure 4: Mesh close-up for Model 3 with total no of 268,164 fine unstructured elements.

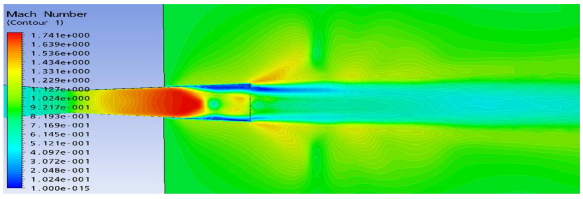

Figure 5: Separation and Lambda shock inside the nozzle NPR 1.78, Model 1.

with comparison to the axisymmetric model NAR 1.5.

Mesh and Solver parameters

After conducting a grid independence test, a medium mesh of 83932 unstructured elements with 45 inflated layers for boundary layer meshing, is used for Model 1 and 187,767 and 268,164 fine unstructured mesh elements with 45 inflated layers, for the Models 2 and 3 was sufficient to capture all flow instabilities. An unstructured mesh was generated using CFX-Mesh, consisting of prisms and hexahedra mesh elements for all three set models. The computational mesh was built in as two body parts as shown in figures 2, 3 and 4 for the respective geometry of Models 1, 2 and 3.

Reynolds number was set to 5.5×10^6 for a Y^+ value equal to 1. The reference length is 22.9mm. Reservoir temperature entering the nozzle inlet is set to 500K while external plume temperature conditions are set to 228K equivalent to 20-22km operating altitude. The walls were specified as adiabatic and no slip. External pressure of 4375Pa is equivalent to 20-22km altitude. Nozzle inlet pressure ratio is varied from 1.27 to 2.4 for low NPRs, and from 4.4 to 12, for high NPRs.

Analysis of separation of the nozzle down stream requires a good model with dual capabilities. Two equation models such as k-ε model k is (Turbulent kinetic energy), ε is (Turbulent dissipation) or k-ω model where ω is (Turbulent frequency) alone, have failed to capture flows subjected to increasing adverse pressure gradients. The Menter's two equation SST model is used for choked nozzle flows under adverse pressure gradient conditions. It offers optimal boundary layer simulation capabilities. Turbulent viscosity is modified to account for transport of the turbulent shear stress. Zonal formulation is a combination based on blending of proper functions of k-ε and k-ω zones without user interaction. SST model shifts values between 1 and 0 of the blending function, F_{sst} to switch from near wall to bulk region [8]. This blending function ensures a smooth transition between k-ε and k-ω models. Shear Stress Transport (SST) turbulence model was used, in ANSYS CFX solver. [7].

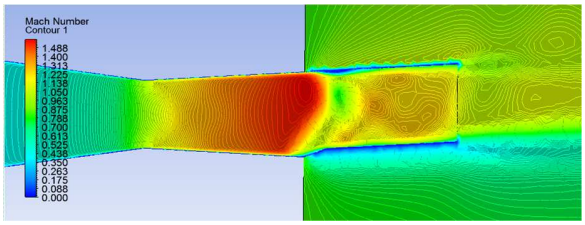

Figure 6: Separation and offset Lambda shock inside the nozzle for NPR 3.4, Model 2.

NPR	(102387Pa) Model 1	(4375Pa) Model 1	(4375Pa) Model 2	(4375Pa) Model 3
4.4	1.8151	2.08225	2.0293	1.9122
5.5	1.8194	2.24133	2.2426	2.1359
7.0	1.8275	2.42494	2.4995	2.4086
10.0	2.4120	2.70229	2.9145	2.7093
12.0	2.1689	2.86748	3.1460	3.0972

Table 1: Mach contours for Models 1(NAR 1.5), 2(NAR 1.14) and 3(NAR 1.21) at 22km.

Results and Conclusions

Flow separation inside the divergent section of the nozzles is shown in figures 5 and 6 for NAR 1.5 and 1.14. Lambda shock formation is visible for model 1 and 2. The internal shock formation takes a different structure for Model 3 (see figure 7) at low NPRs. In figure 8 and 9 the Turbulent kinetic energy dissipation is compared between Models 2 and 3, when the nozzle is highly underexpaned. The energy dissipation of the exhausting gas is markedly different from what we would see in a traditional CD model.

Model	NPR	Force	Plume jet deflection Angle
Model 2	5.5	63.92kN	20.607deg
Model 3	5.5	65.5kN	15.821deg
Model 2	10.0	120.6 kN	30.348 deg
Model 3	10.0	130.2 kN	29.423 deg

Table 2: Steering Thrust for Model 2(NAR 1.14) and 3(NAR 1.21) for NPR 5.5 and 10.0.

Shock formation (4.4< NPR <12) for Model 1, (NAR 1.5) see figures 10 to 13 is compared with Model 2, (NAR 1.14) see figures 14 to 17 and Model 3, (NAR 1.21) see figures 18 to 21. The shock waves become more enlarged as the nozzle pressure is increased, for a given distance of the jet plume region. As the NPR decreases the amount of Mach Diamonds formed within a given distance of the jet plume increase. This could be due to the difference of the ambient pressure at high altitudes and the nozzle exit pressure. The size of the Mach disks and the free jet boundary tend to increase with the increase of NPR (see figures 10 to 17).

Varying the divergent section of the nozzle we see the flow path is vectored away from the axis line. In comparison, the Model 3 Mach contour values are slightly less than in Model 2, see table 1. The flow is significantly offset in the desired direction and is considerably different from the traditional Mach Diamond shock pattern. This variation observed in Model 3, could be implemented to direct the exhaust flow in the desired path in a jet nozzle during sharp turns. Another possible suggestion would be on a missile nozzle, the variation on both top and bottom walls may enhance to vector the thrust when navigating through parabolic trajectories, see figures 18 to 21.

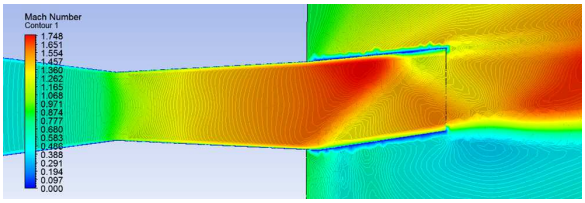

Figure 7: Shock inside the nozzle for NPR 3.4, Model 3.

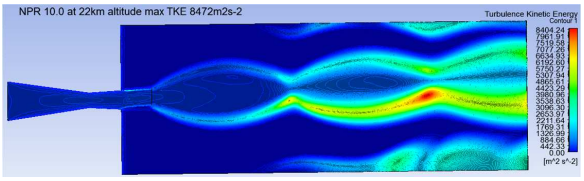

Figure 8: TKE dissipation for NPR 10.0 at 22km, Model 2.

The steering thrust calculations for the Model 2 and 3 are presented on table 2. The deflection jet angle have similar values for both Models for NPR 10.0, while the NPR 5.5 the Model 2 have higher deflection angle in comparison to Model 3. In model 3 with a small divergent variation (8 deg bottom wall) similar deflections can be archived.

Conclusions

Asymmetric nozzle shapes have a major contribution towards the size of the Mach disks and Diamond shock patterns within the jet plume region. Varying the angle of the top and the bottom walls has a significant effect upon the exhaust flow direction. This could be implemented in future high speed nozzles.

References

[1] http://www.pilotfriend.com/training/flight-training/tech/jet-engine-components.htm

[2] http://www.cleveland.com/science/index.ssf/2009/11/clevelands-nasa-glenn-research.html 2010

[3] Mohamed, A., Hamed, A., and Lehnig, T., Supersonic Rectangular Over-Expaned Jets of Single and Two-Phase Flows. ISABE 2003-1119

[4] Xiao, Q., Tsai, H.M., Papamoschou, D. and Johnson, A., Experimental and Numerical study of Jet Mixing from a Shock-Containing Nozzle. AIAA Journal of Propulsion and Power , Vol 25, No 3, May - June 2009.

[5] Xiao, Q., Tsai, H.M. and Papamoschou, D., Numerical Investigation of Supersonic Nozzle Flow Seperation. AIAA Journal, Vol 45, No 3, March 2007.

[6] Menon, N., and Skews, B.W., Rectangular underexpanded gas effects: effect of pressure ratio, aspect ratio and Mach number. Shock Waves 1, Volume 2, 26th Internal Symposium on Shock Waves.

[7] Ekanayake, E.M.S., Gear, J.A., and Ding, Y., Flow simulation of a two dimentional rectangualar supersonic convergent divergent nozzle ANJIAM J. 51 (EMAC2009) pp.C377-C392, 2010.

[8] Menter, F.R., Kuntz, M. and Langtry, R., Ten Years of Industrial Experience with the SST Turbulence Model. Turbulence, Heat and Mass Tranfer 4, 2003.

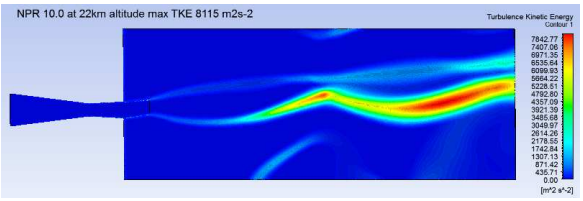

Figure 9: TKE dissipation for NPR 10.0 at 22km, Model 3.

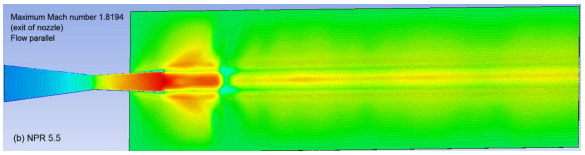

Figure 10: Mach contours for Model 1 at NPR 5.5 at 22km altitude.

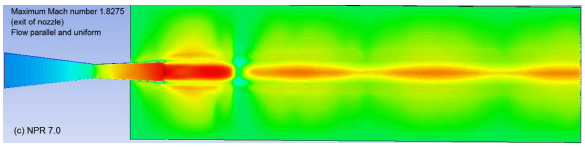

Figure 11: Mach contours for Model 1 at NPR 7.0 at 22km altitude.

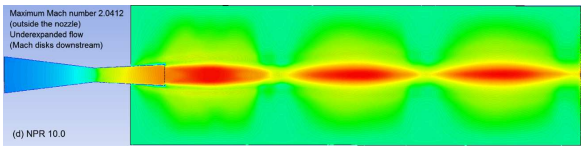

Figure 12: Mach contours for Model 1 at NPR 10.0 at 22km altitude.

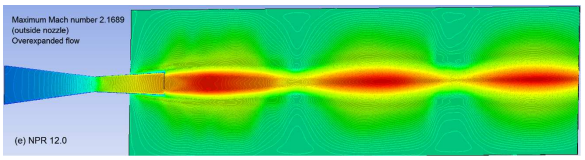

Figure 13: Mach contours for Model 1 at NPR 12.0 at 22km altitude.

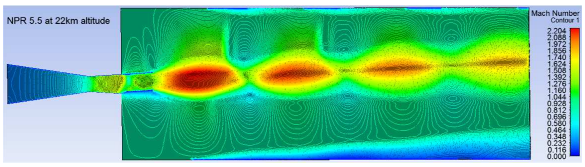

Figure 14: Mach contours for Model 2 at NPR 5.5 at 22km altitude.

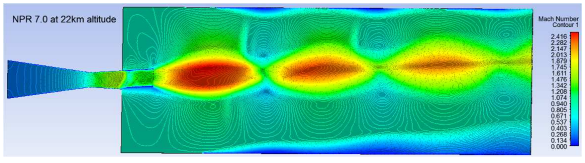

Figure 15: Mach contours for Model 2 at NPR 7.0 at 22km altitude.

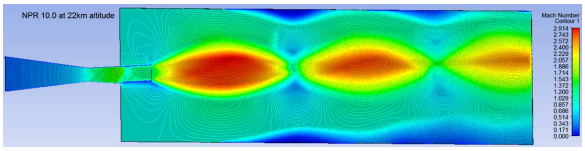

Figure 16: Mach contours for Model 2 at NPR 10.0 at 22km altitude.

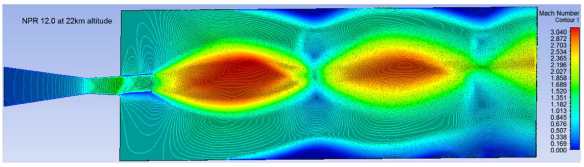

Figure 17: Mach contours for Model 2 at NPR 10.0 at 22km altitude.

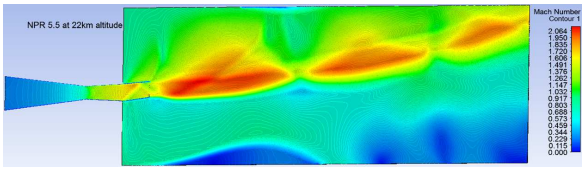

Figure 18: Mach contours for Model 3 at NPR 5.5 at 22km altitude.

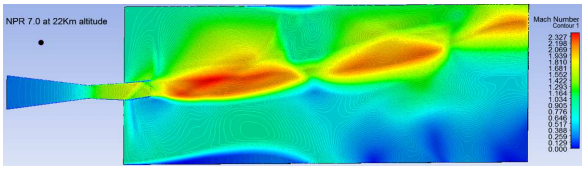

Figure 19: Mach contours for Model 3 at NPR 7.0 at 22km altitude.

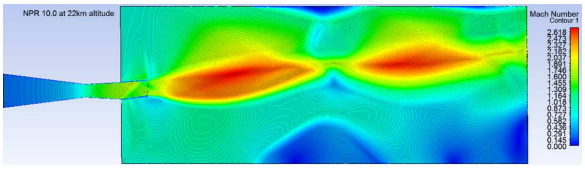

Figure 20: Mach contours for Model 3 at NPR 10.0 at 22km altitude.

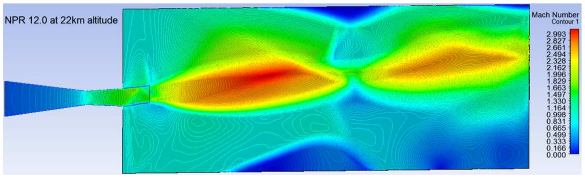

Figure 21: Mach contours for Model 3 at NPR 12.0 at 22km altitude.